Chemical Engineering Journal 381 (2020) 122646

Contents lists available at ScienceDirect

Chemical Engineering Journal

journal homepage: www.elsevier.com/locate/cej

Multiscale investigation of CO_2 hydrate self-sealing potential for carbon geo-sequestration

Jarand Gauteplass[a,b,*], Stian Almenningen[b], Geir Ersland[b], Tanja Barth[a], Jinhai Yang[c], Antonin Chapoy[c]

[a] Department of Chemistry, University of Bergen, Norway
[b] Department of Physics and Technology, University of Bergen, Norway
[c] Institute of Petroleum Engineering, Heriot-Watt University, Edinburgh, UK

HIGHLIGHTS

- CO_2 hydrate reduces the risk of leakage from carbon geo-sequestration.
- Integrity of the CO_2 hydrate seal strongly depends on rock properties.
- Sandstone showed greater potential than limestone for hydrate seal development.
- CO_2 trapped by a combination of pore-spanning hydrate structures and capillary forces.

GRAPHICAL ABSTRACT

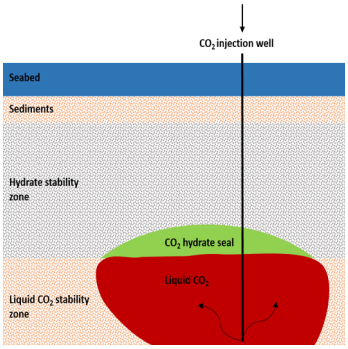

ARTICLE INFO

Keywords:
CO_2 storage
Hydrate seal
Leakage rate
Secondary safety factor
Pore-level visualization

ABSTRACT

Storage of liquid CO_2 in shallow geological formations is a recently proposed concept that can facilitate increased storage capacity and improved mobility control. If stored below the gas hydrate stability zone (GHSZ), unwanted vertical migration of CO_2 can be effectively inhibited by the formation of solid hydrate layers. Lowering the risks of CO_2 leakage to the atmosphere is instrumental to accelerate the implementation of full-scale carbon sequestration in the North Sea and elsewhere.

In the laboratory, we have successfully visualized CO_2 trapping phenomena, measured CO_2 leakage rates, and demonstrated that the integrity of the hydrate seal strongly depends on fluid-rock interactions and initial water distribution. CO_2 propagation in water-filled core samples has been monitored over a total of 140 days inside the GHSZ. Solid CO_2 hydrate formed and sealed the pore space in both homogeneous sandstone and heterogeneous limestone cores. However, the physical flow barrier developed considerably faster in sandstone (after 1.8 pore volumes – PV) compared to limestone (after 7.4 PV), with a factor ten reduced CO_2 leakage rate through the seal in favor of sandstone. Furthermore, pore-scale images of upward CO_2 migration verified trapping of CO_2 both as solid hydrate precipitation and as liquid CO_2 clusters made discontinuous and stabilized by capillary forces. Small-scale hydrate rearrangement followed initial formation, and caused temporarily dissociation of local hydrate structures without affecting the overall integrity of the seal. Our study suggests that a homogeneous, water-filled GHSZ directly above a CO_2 storage site can provide a secondary safety mechanism and significantly reduce the risk of CO_2 leakage.

* Corresponding author at: Department of Chemistry, University of Bergen, Norway.
E-mail address: Jarand.Gauteplass@uib.no (J. Gauteplass).

https://doi.org/10.1016/j.cej.2019.122646
Received 1 July 2019; Received in revised form 26 August 2019; Accepted 27 August 2019
Available online 28 August 2019

1. Introduction

Gas hydrates are naturally occurring clathrates formed in regions of high pressures and low temperatures, i.e. permafrost sediments and deep-sea continental shelves. During formation, water molecules encapsulate small-sized guest molecules such as methane (CH_4) or carbon dioxide (CO_2) in a network of cage-like structures [1]. Agglomeration of solid hydrates within the pore space leads to greatly reduced permeability and blockage of fluid flow [2,3]. Thus, development of flow barriers due to hydrate growth can be utilized as a sealing mechanism for subsurface CO_2 storage and reduce the likelihood of carbon leakage [4]. CO_2 is typically retained in geological formations by structural trapping, capillary trapping, fluid dissolution, and mineral reactions. The importance of each retention method changes over time [5]. Structural and capillary trapping are relevant from the onset of CO_2 injection, whereas the importance of dissolution and especially mineral trapping increases with time. In sediments below deep seabed locations (> 2800 m), CO_2 can also be retained in negative buoyancy zones [6]. The additional trapping mechanism of CO_2 as solid hydrate shows great potential for offshore Europe, where the predicted thickness of the CO_2 hydrate stability zone (HSZ) is nearly 0.5 km of the upper sediments [7]. Gas hydrate in nature (predominately permafrost, feather edge, and subglacial areas) may be a liability to global warming, however, the stability of offshore sedimentary hydrate at the base of the HSZ (CO_2 hydrate seal location) has generally low susceptibility to warming climate [8]. Solid CO_2 hydrate offers a high-density storage alternative to mineral precipitation which often suffers from slow geochemical reaction rates [9]. In contrast, CO_2 hydrate formation is quite fast ($<$ hours) and the kinetics are controlled by the availability of water and the thermal conductivity of the base rock [10]. Hydrate nucleation typically initiates at the fluid interfaces because here guest and water molecules are readily available [11]. Induction time for further massive growth can be long due to slow transport through initial hydrate films at the interfaces [12], and the induction time is also sensitive to the pore size distribution [13]. Increasing the driving forces (e.g. pressure, temperature, chemical potential) evidently accelerates CO_2 hydrate formation [14].

Storage of liquid CO_2 in the upper sediments potentially improves the storage capacity compared to conventional storage of supercritical CO_2 in deep formations. This is because liquid CO_2 is denser than supercritical CO_2, and the solubility of CO_2 in water increases with decreasing temperatures. Because CO_2 is usually transported in a liquid state, it can be injected without having to perform heating operations, and the extra weight in the injection well implies that a lower wellhead pressure is required compared to supercritical CO_2 [15]. Another benefit is the lower buoyancy of liquid CO_2, which reduces gravity segregation and risks of unwanted, upward CO_2 migration [7]. In addition, the macroscopic sweep efficiency increases as liquid CO_2 promotes a more favorable mobility ratio during brine displacement toward a production well [15]. Self-sealing CO_2 storage increases the stability and safety of carbon storage and can accelerate full-scale carbon capture and storage (CCS) deployment. CCS technologies are expected to contribute substantially toward transforming the energy sector and achieving the goals from the Paris Agreement [16]. The technologies target those industrial sectors that will continue to rely on hydrocarbons for decades to come, until renewable energy alternatives are cost-effective and fully competitive. Approximately 2/3 of the current global electricity production remains from fossil fuels [17].

One of the biggest impediment to widespread deployment of CCS is access to geological storage [18]. Therefore, CO_2 hydrate research in porous media is highly relevant because a top-sealing hydrate layer can potentially facilitate carbon storage in areas without known geological traps and cap rocks. Substantial research has been published on the four conventional CO_2 retention mechanisms mentioned above. However, existing research on sedimentary CO_2 hydrate is sparse, with a lot of knowledge gaps related to mechanisms and integrity of CO_2 hydrate seal. Most gas hydrate studies focuses on methane recovery from hydrate dissociation and to some extent from CO_2–CH_4 replacement [19] in geological formations. Forming hydrate layers at the base of the GHSZ as a mean to immobilize and retain upward CO_2 migration is less featured in existing literature. The concept was first presented in 1995 by Koide et al. [20]. Kvamme et al. [21] suggested that liquid transport channels separate hydrate from mineral surfaces, and may serve as distribution channels for CO_2 after initial hydrate formation. Furthermore, Tohidi et al. [22] verified experimentally significant CO_2 retention in hydrate-bearing unconsolidated sand without obvious reduction in permeability. More recently, Massah et al. [23] demonstrated high-density storage of CO_2 hydrate in silica sand (formed in a 5300 cm^3 pressure chamber), and Gauteplass et al. [3] investigated the effect of flow rate, temperature, and salinity on sealing capacity of CO_2 hydrates in consolidated sandstone. Increasing the temperature and salinity, had an adverse effect on formation time of CO_2 hydrate seals, while the effect of flow rate was insignificant in the low flow rate regime. However, others report no measurable effect of salinity on CO_2 hydrate induction time in porous media for certain range of salt concentration [24].

This article presents new insight into self-sealing CO_2 hydrate, particularly highlighting hydrate formation and sealing in multi-porosity and –permeability systems at ultra-low injection rates. To the best of the authors' knowledge, this is the first public research paper investigating the CO_2 hydrate seal potential in carbonates. Direct observations in micromodels complement conventional coreflooding experiments to incorporate pore-level interactions affecting fluid behavior at macro-scale. Micromodels have previously been employed to gain knowledge on pore-level hydrate growth of various guest molecules [25–29] and hydrate dissociation patterns [30,31]. The multiscale approach applied here evaluates the effect of initial water distribution and rock properties on CO_2 hydrate growth pattern and sealing potential.

2. Experimental section

2.1. Coreflooding experiments

Porous media of various properties (detailed in Table 1) were dried, vacuumed, and fully saturated with saline water. Magnetic resonance (MR) images were obtained of the limestone and sandstone cores ex situ to determine the initial water distribution. The superconductive magnet (Bruker BioSpec) has a magnetic field strength of 4.7 T (200 MHz), and the cores were imaged with a spin-echo scan protocol called RAREst (Rapid Acquisition with Relaxation Enhancement with short echo time). Axial two-dimensional slices were positioned uniformly throughout the length of the core, and the voxel resolution was set to $0.5 \times 0.5 \times 10$ mm. The unconsolidated sand pack (average grain size of 256 μm) was prepared by packing layers of dry silica sand grains uniformly within the sleeve by applying a steel piston of constant pressure. The sand column and the end pieces were separated by a

Table 1
Rock, brine, and saturation properties of various porous media used in this study.

	Edwards limestone	Bentheimer sandstone	Silica sand pack
Length, diameter	15.25 cm, 4.83 cm	14.83 cm, 5.12 cm	15.50 cm, 3.82 cm
Pore volume	71 mL	68 mL	72 mL
Porosity (frac.)	0.25	0.22	0.40
Permeability (Abs.)	0.08 D	1.1 D*	0.36 D
Brine composition	3.5 wt% ($CaCl_2$, NaCl)	3.5 wt% (NaCl)	3.5 wt% (NaCl)
Initial saturation	100% brine	100% brine	100% brine

* Value based on statistics from twin core plugs. Not explicitly measured in this study.

double-layered filter (coarse-to-fine) to avoid sand production.

Positioned inside the core holder, the pore volume was stepwise pressurized up to 70 bar with net effective stress of 30 bar. The core temperature was subsequently lowered to 4 °C, moving the system within the gas hydrate stability zone (GHSZ). A schematic of the experimental coreflooding setup is presented in Fig. 1. For consolidated cores, sampling of effluent CO_2 was conducted regularly after hydrate seal formation. Injection of liquid CO_2 was controlled by precise high-pressure pumps (Sanchez Technologies Stigma and Quizix Q5000 series), and a cooling jacket and circulating antifreeze ensured a uniform temperature distribution across the core length. Solid hydrate formation within the pore network occurred for all porous media during steady-state CO_2 injection. Pressure, volume, and temperature measurements were combined to determine the formation of CO_2 hydrates in the opaque system.

2.2. Micromodel experiments

Microfluidic experiments facilitate an excellent platform for direct visualization of pore-level fluid flow and distribution. Qualitative rather than quantitative aspects of such experiments should be highlighted due to the limited volume and number of pores in etched micromodels. A detailed schematic of the micromodel flow rig is shown in Fig. 2. The glass micromodel with etched pore network (68.5 × 5.0 mm) and uniform depth of 50 µm was positioned vertically inside the pressure chamber with main flow direction from bottom to top. The model was carefully pressurized with deionized water to approximately 70 bar (overburden 120 bar) and subsequent cooled by a cryostat (Grant LTC). Methylene blue (0.6 wt%) was added to the water phase for improved visualization and phase identification. The dye is excluded from formation of solid CO_2 hydrates due to molecular size constraints, and does not have any measurable effect on hydrate stability and wettability alterations [25,33]. The water initially occupying the pore space was displaced upward by liquid CO_2 (0.5 mL/hr) followed by hydrate formation. After hydrate formation, the injection mode was switched from constant flow rate to constant pressure of 100 bar, which was controlled by a Quizix pump (Q5000 series). This caused a pressure difference of almost 30 bar across the micromodel. A digital magnifying camera (MOS OPTEM zoom 125) connected to a PC obtained time-lapse images and videos of the field of view inside the pore network. The field of view was illuminated by Meiji Techno fiber optic lite source (FL150). Overburden, temperature, and inlet and outlet pressure were logged during the course of the experiments.

3. Results and discussion

3.1. Hydrate flow barriers

CO_2 migration over a total of 140 days in water-filled porous media of unique porosity, pore-size distribution and permeability were conducted in the laboratory. Interactions of CO_2 and brine at experimental conditions led to formation of solid hydrates, and subsequent build-up of injection pressure in silica sand, in Bentheimer sandstone, and in Edwards limestone material (Fig. 3). Initial hydrate formation occurred after approximately 0.2 PV of CO_2 injected for every core. In the case of unconsolidated silica sand, the initial build-up and collapse of pressure gradient was quickly followed by massive hydrate growth and a significant pressure drop across the sand pack. The hydrate seal was fully developed in the sand pack after 0.6 PV of CO_2 had advanced through the pores. In consolidated Bentheimer sandstone, a modest increase in pressure gradient was temporarily observed at 0.2 PV, however the seal did not fully develop until 1.8 PV of CO_2 was injected. The consolidated Edwards limestone experienced a substantial increase in pressure gradient up until 0.4 PV CO_2 injected, followed by a gradual

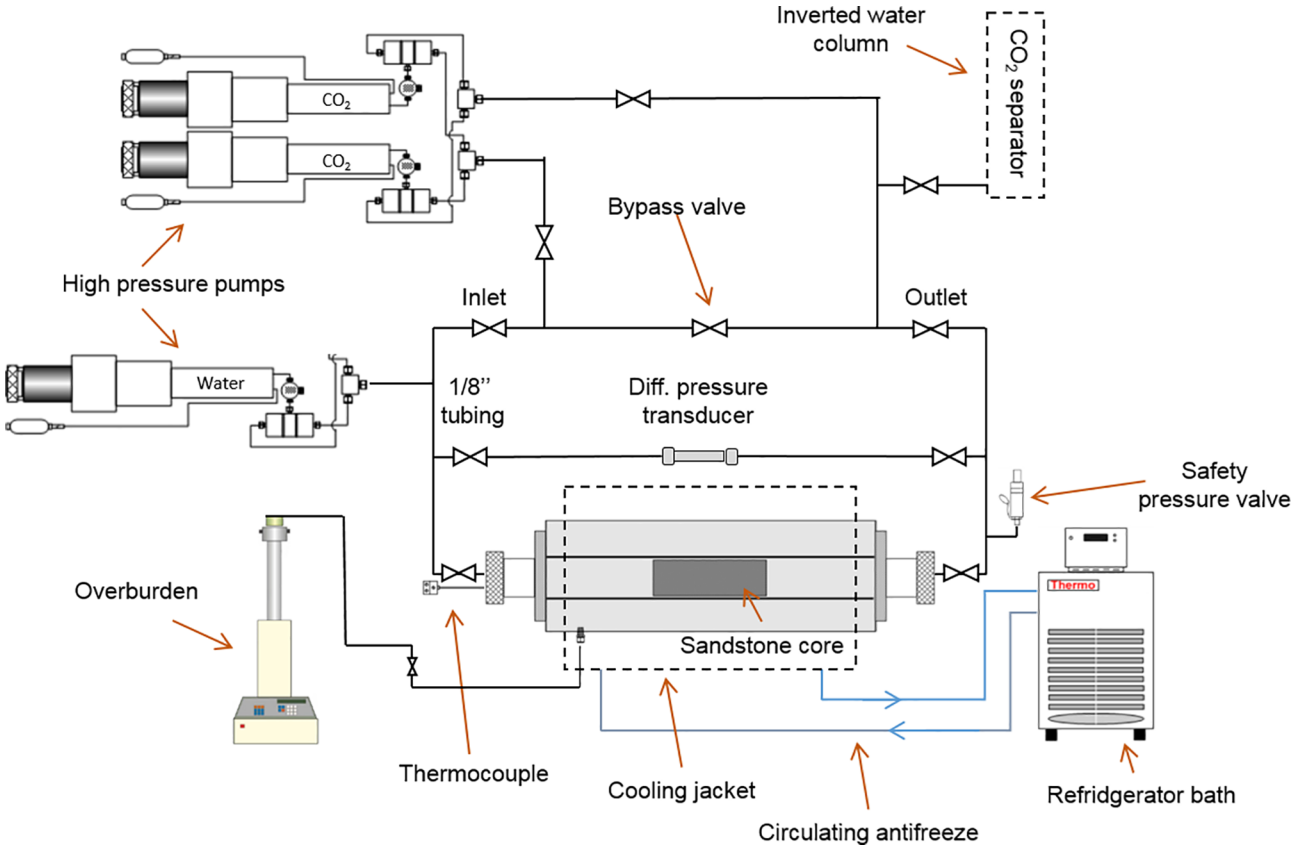

Fig. 1. Coreflooding setup designed for CO_2 hydrate formation at high pressures (70 bar) and low temperatures (4 °C). MR images were obtained ex situ. For consolidated cores, measurements of effluent CO_2 was conducted regularly after hydrate seal formation. Modified from Hågenvik [32].

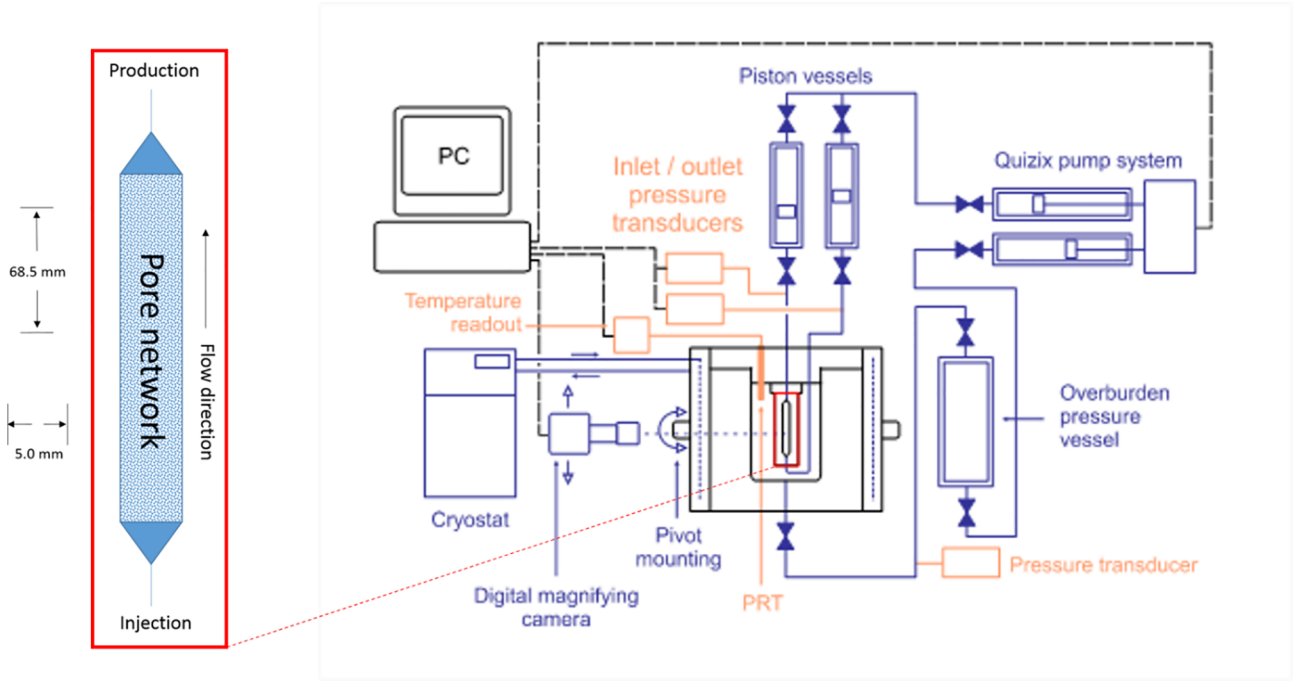

Fig. 2. Glass micromodel with etched pore network (left), and schematic overview of the micromodel rig including cryostat, digital camera with magnifier lens connected to PC, and Quizix Q5000 pump system. The micromodel is positioned vertically within the pressure cell. Modified from Tohidi et al. [34].

reestablishment of injectivity. A total of 7.4 PV of CO_2 was needed to obtain a viscous flow barrier in the limestone core, highlighting a significant increase of volumes CO_2 injected compared to quartz-based porous media. Our results corroborate recent studies on hydrate seal formation in Bentheimer sandstone [3], in tight (0.04 mD) reservoir sandstone [35], and gas permeability effects in hydrate-bearing silica sand [36]. Fast kinetics and short hydrate induction times are instrumental in order to convert upward flow of CO_2 to solid hydrate structures before the migration front escapes the GHSZ and reaches the seabed.

3.2. Quantifying CO_2 escape rates

Once CO_2 hydrate established flow discontinuities through the porous media, a significant pressure drop was imposed by the injection pump (15 bar differential pressure) to demonstrate the robustness of the

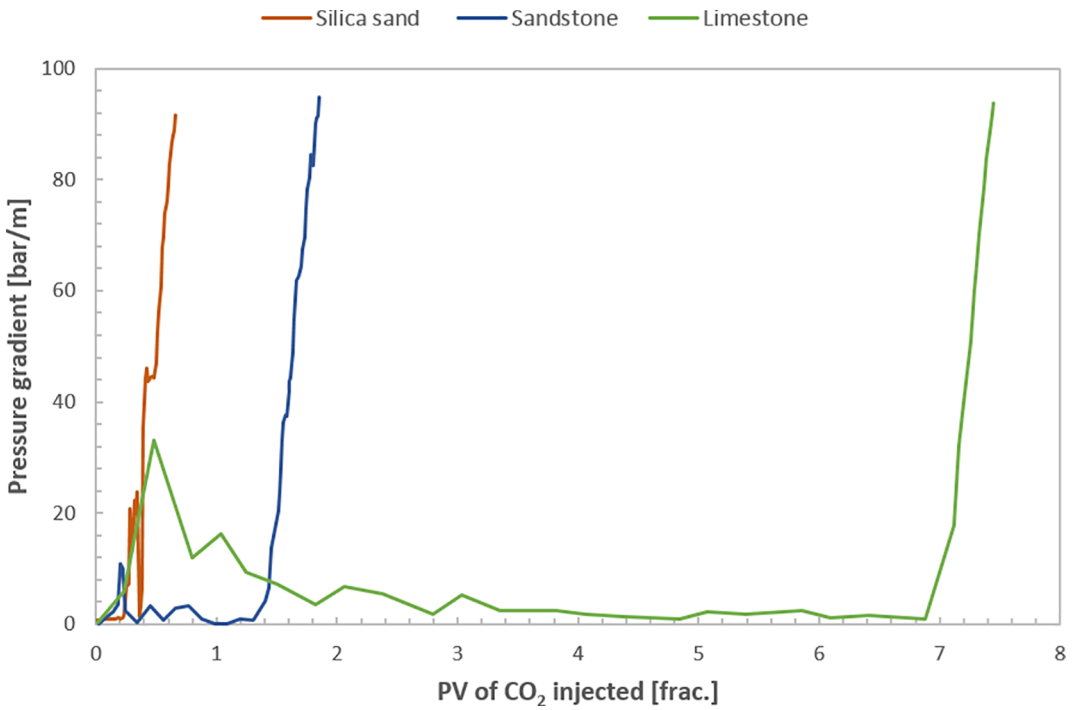

Fig. 3. Development of physical flow barriers in silica sand (0.6 PV), consolidated sandstone (1.8 PV) and consolidated limestone (7.4 PV) from CO_2 hydrate formation. Hydrates formed during continuous CO_2 migration through the pore network. All experiments were conducted at 4 °C and 70 bar, with the pore space initially filled with brine (3.5 wt% salinity). (For interpretation of the references to color in this figure legend, the reader is referred to the web version of this article.)

hydrate seal and compensate for natural pressure decline during conversion of liquid CO_2 to dense CO_2 hydrates. The hydrate seal withstood the stress test (> 80 bar/m) in all of the porous media (Fig. 3.) and showed no sign of bulk structural collapse at current experimental conditions. The consolidated sandstone and limestone cores were further used for investigation of the sealing properties of the formed hydrate layers by quantifying the CO_2 leakage rate across the seals (Table 2 and Fig. 4). After hydrate seal formation (1.8 PV – sandstone, 7.4 PV – limestone), the outlet production line was emptied for CO_2, as breakthrough occurred in both rocks before hydrates formed and sealed off the CO_2 migration paths. Accumulation of CO_2 at the outlet after this point was defined as 'escaped CO_2' and the volume was quantified regularly. The constant pressure drop was maintained during the sampling period. The limestone experiment ran for a total of 47 days, whereas the sandstone ran for 89 days due to a lower initial volumetric injection rate.

Daily CO_2 escape rates through hydrate layers in limestone (green columns) and sandstone (blue columns) are compared directly over a 21-days sampling period in Fig. 4. Though the absolute permeability of limestone (0.08 D) is much lower than sandstone (1.1 D), the CO_2 flow in sandstone was blocked earlier and more efficiently (lower leakage rate) compared to limestone. During the sampling period, seepage of CO_2 through the hydrate seal in sandstone ranged from 0.004 to 0.021 mL/day (average of 0.011 mL/day), whereas in limestone it ranged from 0.068 to 0.163 mL/day (average of 0.103 mL/day). These measurements indicate an order of magnitude higher leakage rate of CO_2 in limestone compared to sandstone. This pattern is consistent for every measuring period, and demonstrates a significant difference in hydrate sealing capacity in quartz-dominated versus calcite-dominated porous media. Furthermore, at 51 days after the hydrate barrier developed (not shown in Fig. 4), the CO_2 seepage rate stabilized at a reduced rate of 0.001 mL/day for the next 20 days in sandstone. Because the limestone experiment was ended 40 days after hydrate barrier formation, no sampling data is available for comparison to additional CO_2 escape rate reduction in sandstone. Focus should therefore be on the sampling period from 19 to 40 days after hydrate formation, where the two experiments are directly comparable and hydrate induction time is accounted for. However, based on the limestone trend line in Fig. 4, there are no indications of a sudden decrease in CO_2 seepage rate at current conditions.

The ability of solid hydrates to seal CO_2 migration paths in porous media depends on several parameters, including rock properties (mineral composition, pore-size distribution, wettability), and fluid properties (composition, saturation, distribution). Even though both media were initially 100% saturated with water prior to CO_2 injection, the pore connectivity caused the water distribution within the cores to vary significantly, as demonstrated in Fig. 5. Here, axial MR images are obtained from sandstone (left) and limestone (right) at fractional lengths L = 0.5 (middle) and L = 0.8 (outlet). Signal intensity is displayed in grey scale and areas of high water saturation (large pores) correlates with bright pixels. Initial water distribution in sandstone appears consistent in both the axial and longitudinal plane as opposed to limestone. In the heterogeneous limestone, large water-filled pores appear scattered and poorly connected. Dark pixels represents areas of minerals and micro pores where hydrate formation is unlikely due to severe capillary threshold pressures. CO_2 invasion in predominately large pores is followed by hydrate formation in areas where both phases are readily available. This facilitates development of a continuous hydrate seal in homogeneous sandstone pores, in contrast to a fragmented hydrate seal in heterogeneous limestone pores, based on the obtained MR images.

While formation of hydrate seals the pore space by reducing the effective porosity, mineral dissolution processes have the opposite effect. Carbonate materials are highly reactive in a CO_2-water system [37]. Limestone dissolution can cause substantial permeability and porosity increase [38], hence creating new potential CO_2 escape paths. Increase in local porosity due to dissolution in Edward limestone is shown in Fig. 6, by comparing pre- and post-experimental MR images. Axial water signal intensity (bright pixels) increased by a factor of 1.5 (at length 0.35) and by a factor of 2.4 (L = 0.43), highlighted with box A and B. In addition to interior porosity increase, mineral dissolution led to a substantial cavity on the core surface (box C). These microstructural changes further increased the number of CO_2 flow channels in the carbonate pore network. If availability of water is restrained in the newly formed channels, CO_2 hydrates cannot successfully form and seal off this zone. The combination of heterogeneous water distribution and local mineral dissolution is likely the main reason why CO_2 leakage rates were an order of magnitude higher in limestone than in sandstone. Dissolution processes after formation of hydrates were hampered by hydrate barriers blocking transportation of dissolved Ca^{2+} through the core sample.

In general, untreated (not aged with crude oil) sandstone and limestone cores are strongly water-wet in a CO_2-water system [39]. However, wettability alterations have been reported using supercritical CO_2 at high temperature and pressure in quartz [40], and at high salinity and pressure (200 bar) in calcite [41]. We simulate offshore shallow aquifer conditions in this paper using liquid CO_2, low temperatures and salinities, and moderate pressures. These conditions presumably make our sandstone and carbonate samples maintain their hydrophilic mineral surfaces and strongly water-wet properties throughout the experiments. Though the surface charge is opposite in the two cores due to the different mineral composition, water will still distribute itself along grain surfaces and in smaller pores, whereas non-wetting CO_2 will occupy the center of larger pores when overcoming the capillary threshold pressure. Furthermore, the activity of water molecules adjacent to mineral surfaces are lower compared to water molecules in the center of pores [42]. The reduced activity of water molecules implies that wetting films are preserved after hydrate formation, and may act as escape routes [21,25,42]. To investigate pore-level trapping mechanisms and fluid distribution channels, micromodels serving as an analogue to three-dimensional rocks were studied in the following section.

3.3. Pore-level CO_2 hydrate mechanisms

Direct visualization of upward CO_2 migration in a glass micromodel verified CO_2 trapping by hydrate formation. The initial CO_2 flow path was efficiently made discontinuous and the phase immobilized as CO_2 and water gradually converted to solid hydrate in the pore network (Fig. 7), resulting in a significant increase in inlet pressure. The injection pump was eventually set to constant pressure equal to 100 bar after 86 min, and the integrity of the hydrate seal was maintained throughout the experiment. The insets in Fig. 7 show preferred CO_2 (red color) flow paths after draining the water phase (blue color) from the largest pores in an upward direction. In such a flow regime, capillary

Table 2
Comparison of CO_2 sealing properties in carbonate and sandstone.

	Edwards limestone	Bentheimer sandstone
Pressure, Temperature	70 bar, 4 °C	70 bar, 4 °C
Flow rate	0.05 mL/min	0.005 mL/min
Hydrate barrier developed	After 7.4 PV inj (7 days)	After 1.8 PV inj (17 days)
Rate of escaped CO_2 (average)	0.10* mL/day	0.011* mL/day
Sampling period	21 days	21 days
Length of experiment	47 days	89 days
Total amount of CO_2 injected	631 mL	259 mL

* The original values measured at standard temperature and pressure conditions have been converted to experimental conditions by simple density calculations. The relative CO_2 escape rate (tenfold increase) relation should be highlighted rather than the absolute values.

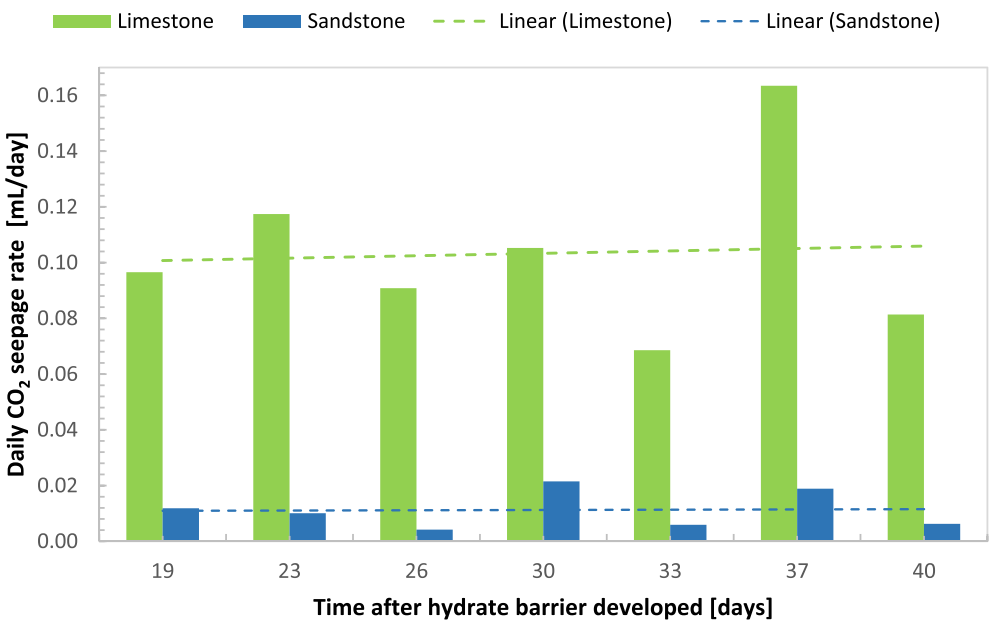

Fig. 4. Rate of CO_2 escaping the hydrate seal of respectively Edwards limestone and Bentheimer sandstone. The measured rate (mL/day) is averaged over the time period of sampling. Linear trend lines indicate average CO_2 escape rates of 0.10 mL/day (limestone) and 0.011 mL/day (sandstone) for the 21 days sample period. Both experiments were conducted at 4 °C and 70 bar, and with 3.5 wt% brine salinity. (For interpretation of the references to color in this figure legend, the reader is referred to the web version of this article.)

forces dominate the pore occupancy and filling sequences [43]. Some redistribution occurred in the network, where initial CO_2 migration paths were redirected by local snap-off events. These shifts led to capillary trapped CO_2 surrounded by water-filled pore throats. Hydrate growth (grey color) appeared uniformly throughout the network, rather than as a distinct hydrate front advancing through the pore space. Conversion to solid hydrates occurred predominately in larger pores initially occupied by liquid CO_2. The liquid CO_2 saturation effectively decreased during hydrate formation and the remaining liquid CO_2 was located in the upper production channel and in a few large pores in the model. A combination of pore-spanning hydrate layers and strong capillary forces stabilized the isolated pockets of liquid CO_2. The micro-visual data showed no sign of viscous displacement or substantial film flow after hydrate seal formation. The limiting fluid phase in the system is water, however full conversion of water to hydrate was not observed. Water, liquid CO_2 and hydrates co-existed due to lack of available host/guest molecules at the current locations. The formed CO_2 hydrate effectively shielded the remaining pore water and inhibited further growth. However, with time, molecular diffusion causes the free water to be fully saturated with CO_2. Substantial hydrate nucleation from CO_2 dissolved in water has been experimentally verified at similar conditions [44].

CO_2 hydrates precipitated in pores of various geometrical shapes and sizes. Initial formation in pores occupied by liquid CO_2 was soon followed by formation in smaller water-filled pores and pore-throats, where the induction time is typically longer [13]. On the scale of days the hydrate morphology changed from a dark, coarse opaque filling to higher degree of transparency due to rearrangement of the hydrate crystals [27]. Ostwald ripening stabilized the maturing hydrate structure [45,46]. Agglomeration of individual hydrate fronts took place, driven by the minimization of energy and surface-to-volume ratio. Massive hydrates spanned entire pore diameters without evidence of preserved water films (> 10 μm thickness) at current resolution. Hydrates appeared pore-filling as well as cementing within the field of view. However, shadowing effects near the pore walls may mask thin water films between grains and hydrate, as visualized at pore-scale [25,47]. In the upper production channel, hydrates were distributed as layers along the pore walls with liquid CO_2 occupying the center. This CO_2 was not converted to hydrates for the time investigated because of halted water supply.

The pressure drop imposed by the injection pump was maintained at 25 bar for several days during continuous visual monitoring. Fig. 8 shows evidence of small-scale hydrate dissociation at specific locations within the porous network (marked with red rings). The right image was obtained three days later under identical conditions. The dissociation temperature for the system was experimentally and

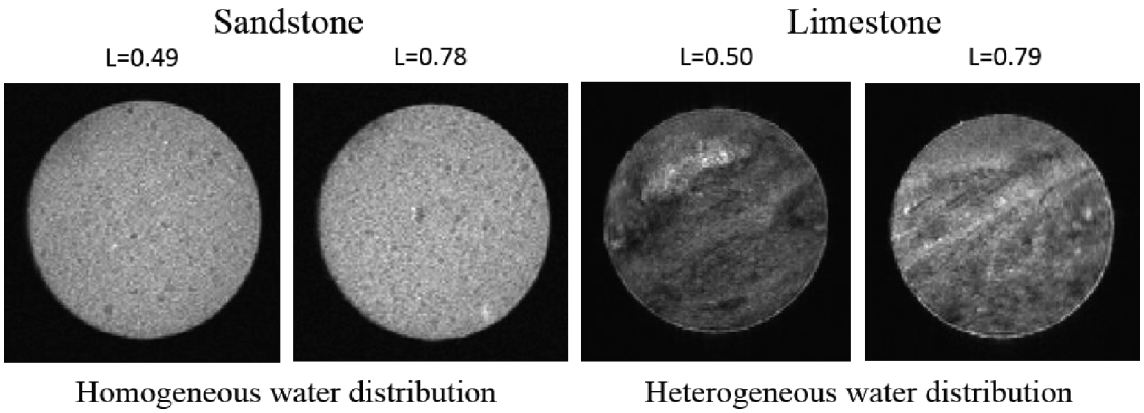

Fig. 5. Axial MR images (0.5 × 0.5 × 10 mm voxel resolution) of Bentheimer sandstone (left) and Edwards limestone (right) at two fractional core lengths obtained prior to CO_2 injection. Signal intensity is displayed in grey scale and areas of high water saturation correlates with bright pixels. Pore sizes and initial water distribution in the sandstone appears consistent in both the axial and longitudinal plane as opposed to the limestone core.

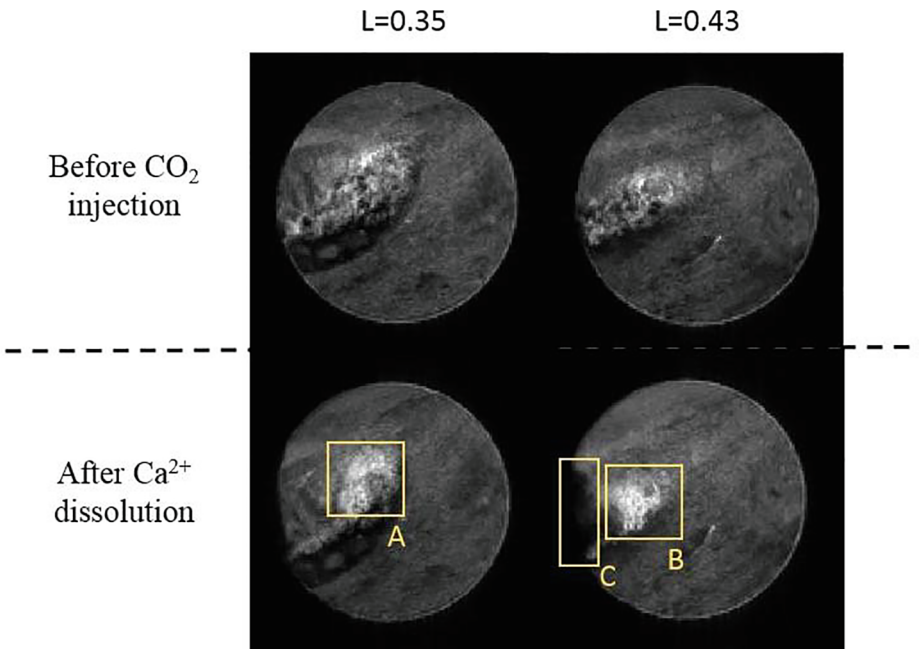

Fig. 6. Before and after images (0.5 × 0.5 × 10 mm voxel resolution) of CO_2 injection in Edwards limestone obtained by MRI. Mineral dissolution by the CO_2/brine solution led to large vugs to the left in the cross-sections resulting in areas of increased water saturation (box A and B) and completely dissolved limestone (box C) leaving a substantial cavity on the core surface. The lower images were obtained after the CO_2 experiment ended, and the sample had been re-saturated with 100% water to gain high signal intensity.

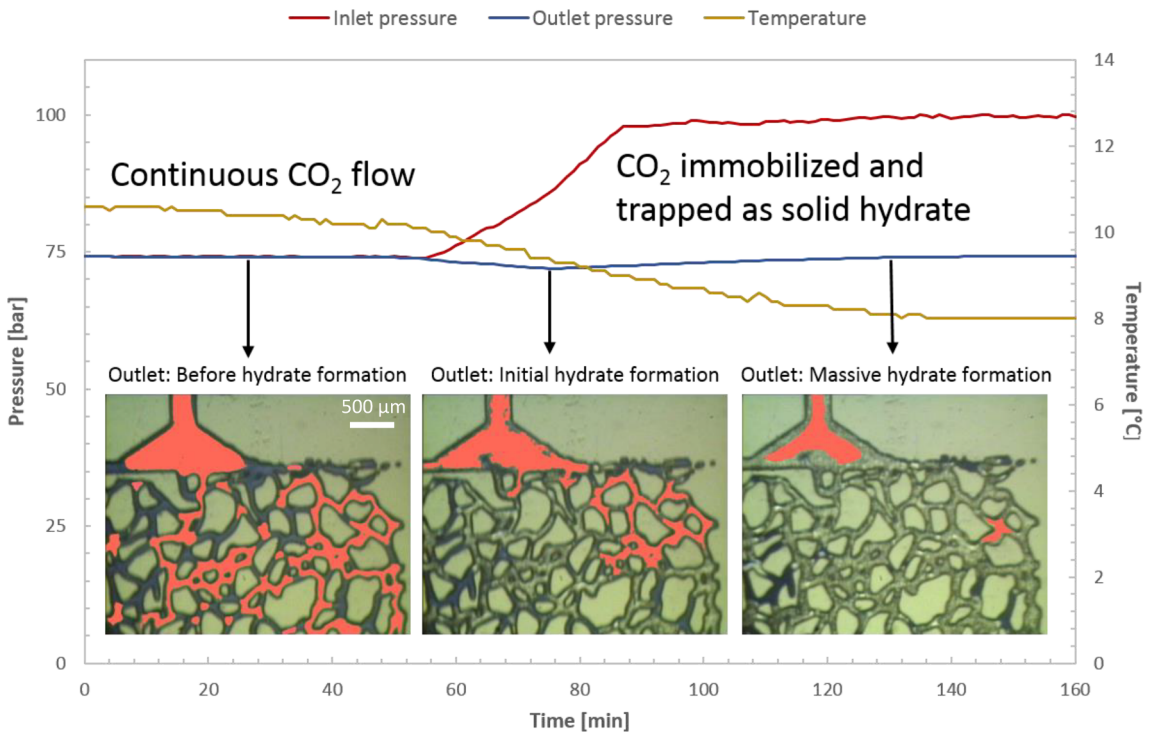

Fig. 7. Verification of pore-level CO_2 trapping. Inlet pressure increased during upward CO_2 migration as hydrates formed and blocked CO_2 flow paths in the pore network. Insets: Stepwise isolation and immobilization of CO_2 during hydrate formation (red color = liqCO_2, blue = water, grey = hydrate). (For interpretation of the references to color in this figure legend, the reader is referred to the web version of this article.)

numerically verified to be 2.0–2.5 °C higher than the current temperature. The few observations of local hydrate dissociation are believed to be part of gradual hydrate redistribution, with associated reformation at nearby places. Large and well-organized hydrate crystals grow at the expense of smaller crystals, and CO_2 and water are temporarily released through this rearrangement process. The inherent self-preserving property of hydrates [48] slowed further dissociation. The limited hydrate dissociation did not result in viscous mobilization of released CO_2 in pores due to high capillary threshold pressures and interstitial hydrate layers. Over time, hydrate re-formation of the liberated fluids will occur due to the favorable thermodynamic properties promoting stability. The dissociation of local hydrate structures and following hydrate formation had no measurable effect on the overall integrity of the solid hydrate seal under current conditions.

4. Conclusions

We have shown that the integrity of the CO_2 hydrate seal strongly depends on rock properties. Hydrate formed physical migration barriers in both consolidated and unconsolidated media, and the barriers

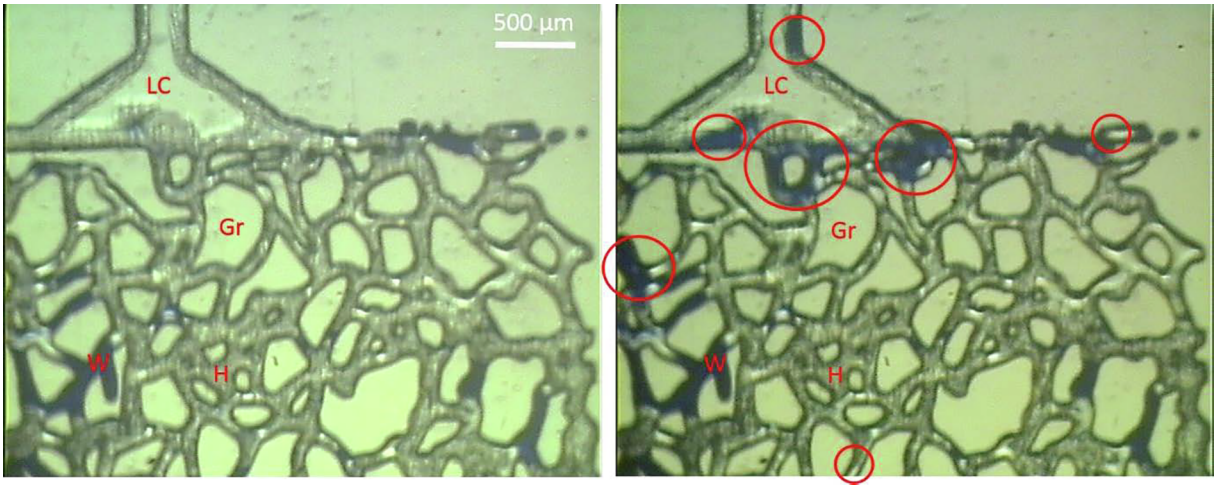

Fig. 8. Visual observations of local CO_2 hydrate dissociation with differential pressure of 25 bar and temperature equal to 8 °C. The left image was captured following the formation of the hydrate seal, whereas the right image is captured three days later under identical conditions. Red circles show specific areas of release of free water and liquid CO_2. The liquid CO_2 was trapped by capillary forces and interstitial hydrate layers, and the local hydrate dissociation did not affect the overall integrity of the CO_2 hydrate seal. Legends: Gr = Grains, LC = Liquid CO_2, W = Water, H = Hydrate. (For interpretation of the references to color in this figure legend, the reader is referred to the web version of this article.)

withstood significant pressure drops. However, the hydrate seal developed faster in sandstone than limestone, with a factor ten reduction in CO_2 leakage rate through the seal in favor of the sandstone. We believe this discrepancy in seal integrity can be ascribed to heterogeneous initial water (pore size) distribution and mineral dissolution in limestone, as supported by MRI data. Formation of vugs/wormholes in CO_2 invaded limestone pores, increased the effective porosity and the number of potential CO_2 escape channels. In sandstone where rock-fluid reactions were not observed, the CO_2 leakage rate was significantly reduced after 51 days of hydrate sealing, and remained constant for the rest of the measurements (20 additional days). Furthermore, pore-scale images of upward CO_2 migration verified trapping of CO_2 both as solid hydrate precipitation and as discontinuous liquid CO_2 clusters stabilized by capillary forces. Water, liquid CO_2, and hydrate phases were all observed to co-exist in pores within the GHSZ for the time investigated. Small-scale hydrate rearrangement followed initial formation, and caused temporarily dissociation of local hydrate structures without affecting the overall integrity of the seal. Our findings support higher CO_2 retention rates through hydrate layers in sandstone than limestone, and that CO_2 is immobilized by a combination of pore-spanning hydrate layers and capillary threshold in hydrophilic pore networks. If rock-fluid reactions are limited, a water-filled GHSZ directly above a CO_2 storage site can provide a secondary safety mechanism and significantly reduce the risk of CO_2 leakage toward the seabed and the atmosphere.

Acknowledgements

We gratefully acknowledge Equinor for access to MRI facilities in Bergen, Norway and financial support by the Research Council of Norway [grant number 255490] and by the Academia-agreement between Equinor and the University of Bergen.

References

[1] E.D. Sloan, Gas hydrates: review of physical/chemical properties, Energy Fuels 12 (2) (1998) 191–196.
[2] A.I. Evrenos, J.K. Heathman, J. Ralstin, Impermeation of porous media by forming hydrates in situ, J. Petrol. Technol. (1971.) 23(09).
[3] J. Gauteplass, S. Almenningen, G. Ersland, T. Barth, Hydrate seal formation during laboratory CO2 injection in a cold aquifer, Int. J. Greenhouse Gas Control 78 (2018) 21–26.
[4] H. Koide, M. Takahashi, Y. Shindo, Y. Tazaki, M. Iijima, K. Ito, N. Kimura, K. Omata, Hydrate formation in sediments in the sub-seabed disposal of CO2, Energy 22 (2) (1997) 279–283.
[5] S. Benson, D.R. Cole, CO2 sequestration in deep sedimentary formations, Elements 4 (5) (2008) 325–331.
[6] F. Qanbari, M. Pooladi-Darvish, S. Hamed Tabatabaie, S. Gerami, Storage of CO2 as hydrate beneath the ocean floor, Energy Procedia 4 (2011) 3997–4004.
[7] C.A. Rochelle, A.P. Camps, D. Long, A. Milodowski, K. Bateman, D. Gunn, P. Jackson, M.A. Lovell, J. Rees, Can CO2 hydrate assist in the underground storage of carbon dioxide? Geol. Soc., London, Special Publications 319 (1) (2009) 171–183.
[8] C.D. Ruppel, J.D. Kessler, The interaction of climate change and methane hydrates, Rev. Geophys. 55 (1) (2017) 126–168.
[9] W.D. Gunter, B. Wiwehar, E.H. Perkins, Aquifer disposal of CO2-rich greenhouse gases: extension of the time scale of experiment for CO2-sequestering reactions by geochemical modelling, Mineral. Petrol. 59 (1) (1997) 121–140.
[10] O.Y. Zatsepina, M. Pooladi-Darvish, Storage of CO2 hydrate in shallow gas reservoirs: pre- and post-injection periods, Greenhouse Gases Sci. Technol. 1 (3) (2011) 223–236.
[11] A.V. Palodkar, A.K. Jana, Formulating formation mechanism of natural gas hydrates, Sci. Rep. 7 (1) (2017) 6392.
[12] B. Kvamme, S.A. Aromada, N. Saeidi, Heterogeneous and homogeneous hydrate nucleation in CO2/water systems, J. Cryst. Growth 522 (2019) 160–174.
[13] X. Zhang, J. Li, Q. Wu, C. Wang, J. Nan, Experimental study on the effect of pore size on carbon dioxide hydrate formation and storage in porous media, J. Nat. Gas Sci. Eng. 25 (2015) 297–302.
[14] S.-P. Kang, J.-W. Lee, Kinetic behaviors of CO2 hydrates in porous media and effect of kinetic promoter on the formation kinetics, Chem. Eng. Sci. 65 (5) (2010) 1840–1845.
[15] V. Vilarrasa, O. Silva, J. Carrera, S. Olivella, Liquid CO2 injection for geological storage in deep saline aquifers, Int. J. Greenhouse Gas Control 14 (Supplement C) (2013) 84–96.
[16] P. Ekins, N. Hughes, S. Pye, M. Winning, R. Macrory, B. Milligan, S. Haszeldine, J. Watson, The role of CCS in meeting climate policy targets, 2017, Report by the UCL Institute for Sustainable Resources, p. 150.
[17] EASAC, Negative emission technologies: What role in meeting Paris Agreement targets? 2018, EASAC policy report 35. p. 39.
[18] OECD/IEA, 20 Years of Carbon Capture and Storage – Accelerating Future Deployment, International Energy Agency, 2016.
[19] G. Ersland, J. Husebø, A. Graue, B.A. Baldwin, J. Howard, J. Stevens, Measuring gas hydrate formation and exchange with CO2 in Bentheim sandstone using MRI tomography, Chem. Eng. J. 158 (1) (2010) 25–31.
[20] H. Koide, M. Takahashi, H. Tsukamoto, Y. Shindo, Self-trapping mechanisms of carbon dioxide in the aquifer disposal, Energy Convers. Manage. 36 (6) (1995) 505–508.
[21] B. Kvamme, A. Graue, T. Buanes, T. Kuznetsova, G. Ersland, Storage of CO2 in natural gas hydrate reservoirs and the effect of hydrate as an extra sealing in cold aquifers, Int. J. Greenhouse Gas Control 1 (2) (2007) 236–246.
[22] B. Tohidi, J. Yang, M. Salehabadi, R. Anderson, A. Chapoy, CO2 hydrates could provide secondary safety factor in subsurface sequestration of CO2, Environ. Sci. Technol. 44 (4) (2010) 1509–1514.
[23] M. Massah, D. Sun, H. Sharifi, P. Englezos, Demonstration of gas-hydrate assisted carbon dioxide storage through horizontal injection in lab-scale reservoir, J. Chem. Thermodyn. 117 (2018) 106–112.
[24] S.H.B. Yang, P. Babu, S.F.S. Chua, P. Linga, Carbon dioxide hydrate kinetics in porous media with and without salts, Appl. Energy 162 (2016) 1131–1140.
[25] B. Tohidi, R. Anderson, B. Clennell, R.W. Burgass, A. Biderkab, Visual observation of gas-hydrate formation and dissociation in synthetic porous media by means of

glass micromodels, Geology 29 (9) (2001) 867–870.
[26] D. Katsuki, R. Ohmura, T. Ebinuma, H. Narita, Formation, growth and ageing of clathrate hydrate crystals in a porous medium, Philos. Mag. 86 (12) (2006) 1753–1761.
[27] L.P. Hauge, J. Gauteplass, M.D. Høyland, G. Ersland, A. Kovscek, M.A. Fernø, Pore-level hydrate formation mechanisms using realistic rock structures in high-pressure silicon micromodels, Int. J. Greenhouse Gas Control 53 (2016) 178–186.
[28] S. Almenningen, J. Flatlandsmo, A.R. Kovscek, G. Ersland, M.A. Ferno, Determination of pore-scale hydrate phase equilibria in sediments using lab-on-a-chip technology, Lab Chip (2017).
[29] M. Muraoka, Y. Yamamoto, In situ chamber built for clarifying the relationship between methane hydrate crystal morphology and gas permeability in a thin glass micromodel cell, Rev. Sci. Instrum. 88 (6) (2017) 064503.
[30] D. Katsuki, R. Ohmura, T. Ebinuma, H. Narita, Visual observation of dissociation of methane hydrate crystals in a glass micro model: production and transfer of methane, J. Appl. Phys. 104 (8) (2008) 083514.
[31] S. Almenningen, E. Iden, M.A. Fernø, G. Ersland, Salinity effects on pore-scale methane gas hydrate dissociation, J. Geophys. Res. Solid Earth 123 (7) (2018) 5599–5608.
[32] C. Hågenvik, CO2 Injection in Hydrate Bearing Sandstone with Excess Water, University of Bergen, 2013, p. 117.
[33] M. Sohrabi, A. Danesh, D.H. Tehrani, M. Jamiolahmady, Microscopic mechanisms of oil recovery by near-miscible gas injection, Transp. Porous Media 72 (3) (2008) 351–367.
[34] B. Tohidi, R. Anderson, B. Clennell, J. Yang, A. Bashir, R.W. Burgess, Application of high pressure glass micromodels to gas hydrate studies, International Conference on Gas Hydrates – 4, Yokohama, 2002.
[35] S. Almenningen, P. Betlem, A. Hussain, S. Roy, K. Senger, G. Ersland, Demonstrating the potential of CO2 hydrate self-sealing in Svalbard, Arctic Norway, Int. J. Greenhouse Gas Control 89 (2019) 1–8.
[36] A. Okwananke, A. Hassanpouryouzband, M. Vasheghani Farahani, J. Yang, B. Tohidi, E. Chuvilin, V. Istomin, B. Bukhanov, Methane recovery from gas hydrate-bearing sediments: an experimental study on the gas permeation characteristics under varying pressure, J. Petrol. Sci. Eng. 180 (2019) 435–444.
[37] A.R. Lawter, N.P. Qafoku, R.M. Asmussen, D.H. Bacon, L. Zheng, C.F. Brown, Risk of geologic sequestration of CO2 to groundwater aquifers: current knowledge and remaining questions, Energy Procedia 114 (2017) 3052–3059.
[38] C. Noiriel, P. Gouze, D. Bernard, Investigation of porosity and permeability effects from microstructure changes during limestone dissolution, Geophys. Res. Lett. (24) (2004) 31.
[39] S. Iglauer, C.H. Pentland, A. Busch, CO2 wettability of seal and reservoir rocks and the implications for carbon geo-sequestration, Water Resour. Res. 51 (1) (2015) 729–774.
[40] S. Saraji, L. Goual, M. Piri, H. Plancher, Wettability of supercritical carbon dioxide/water/quartz systems: simultaneous measurement of contact angle and interfacial tension at reservoir conditions, Langmuir 29 (23) (2013) 6856–6866.
[41] M. Arif, M. Lebedev, A. Barifcani, S. Iglauer, CO2 storage in carbonates: wettability of calcite, Int. J. Greenhouse Gas Control 62 (2017) 113–121.
[42] M.B. Clennell, M. Hovland, J.S. Booth, P. Henry, W.J. Winters, Formation of natural gas hydrates in marine sediments: 1. Conceptual model of gas hydrate growth conditioned by host sediment properties, J. Geophys. Res.: Solid Earth 104 (B10) (1999) 22985–23003.
[43] J. Gauteplass, H. Follesø, A. Graue, A. Kovscek, M.A. Fernø, Visualization of pore-level displacement mechanisms during CO2 injection and EOR processes, EAGE IOR 2013 – 17th European Symposium on Improved Oil Recovery, St. Petersburg, Russia, (2013).
[44] S. Almenningen, J. Gauteplass, P. Fotland, G.L. Aastveit, T. Barth, G. Ersland, Visualization of hydrate formation during CO2 storage in water-saturated sandstone, Int. J. Greenhouse Gas Control 79 (2018) 272–278.
[45] M. Chaouachi, S.H. Neher, A. Falenty, W.F. Kuhs, Time resolved coarsening of clathrate crystals: the case of gas hydrates, Cryst. Growth Des. 17 (5) (2017) 2458–2472.
[46] X. Chen, D.N. Espinoza, Ostwald ripening changes the pore habit and spatial variability of clathrate hydrate, Fuel 214 (2018) 614–622.
[47] D. Sadeq, S. Iglauer, M. Lebedev, T. Rahman, Y. Zhang, A. Barifcani, Experimental pore-scale analysis of carbon dioxide hydrate in sandstone via X-Ray micro-computed tomography, Int. J. Greenhouse Gas Control 79 (2018) 73–82.
[48] T.-H. Kwon, G.-C. Cho, J.C. Santamarina, Gas hydrate dissociation in sediments: pressure-temperature evolution, Geochem. Geophys. Geosyst. (3) (2008) 9.